Accepted Manuscript

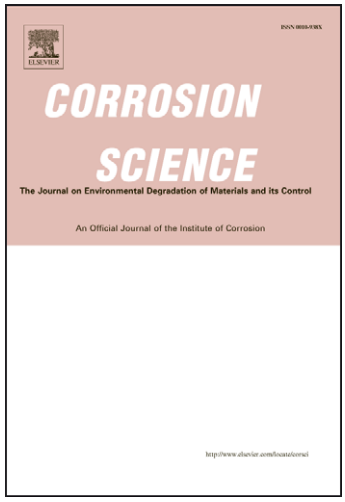

The effect of temperature and concentration on the corrosion inhibition mechanism of an amphiphilic amido-amine in CO_2 saturated solution

M.P. Desimone, G. Gordillo, S.N. Simison

PII: S0010-938X(11)00422-7
DOI: 10.1016/j.corsci.2011.08.009
Reference: CS 4571

To appear in: *Corrosion Science*

Received Date: 10 May 2011
Accepted Date: 4 August 2011

Please cite this article as: M.P. Desimone, G. Gordillo, S.N. Simison, The effect of temperature and concentration on the corrosion inhibition mechanism of an amphiphilic amido-amine in CO_2 saturated solution, *Corrosion Science* (2011), doi: 10.1016/j.corsci.2011.08.009

The effect of temperature and concentration on the corrosion inhibition mechanism of an amphiphilic amido-amine in CO_2 saturated solution

M. P. Desimone[1], G. Gordillo[2], S. N. Simison[1]

1- División Corrosión, INTEMA-CONICET, UNMdP, Juan B. Justo 4302, B7608FDQ, Mar del Plata, Argentina.

2- INQUIMAE (CONICET) - DQIAQF – Facultad de Ciencias Exactas y Naturales, Universidad de Buenos Aires, Ciudad Universitaria, Pabellón 2, Buenos Aires, Argentina.

Abstract

The corrosion inhibition mechanism of the N-[2-[(2-aminoethyl)amino]thyl]-9-octadecenamide on mild steel surface in CO_2-saturated 5% NaCl solution has been studied. The inhibition efficiency decreases with increasing temperature. Adsorption of the inhibitor studied is found to follow the Frumkin adsorption isotherm. EIS results show that the mechanism of its corrosion inhibition at concentrations higher than critical micelle concentration is by forming a protective porous bi-layer. The activation energy, thermodynamic parameters and electrochemical results reveal a change in the adsorption mode of the inhibitor studied: the inhibitor could primarily be physically adsorbed at low concentrations, while chemisorption is favoured as concentration increases.

Keywords: A. Mild steel; B. EIS; C. CO_2 corrosion; C. Thermodynamic characterization; C. Frumkin isotherm.

1. Introduction

Carbon steels are the most commonly used construction materials for pipelines in the oil and gas industry but they are very susceptible of both a high general corrosion rate and severe localized corrosion [1]. CO_2 corrosion is one of the most significant causes in the oil and gas pipelines failures and occurs at all stages of production from downhole to surface equipment and processing facilities [2, 3]. Carbon dioxide gas dissolves into the saltwater and forms weak carbonic acid. This acid reacts with the iron of the carbon steel pipes enhancing their corrosion rate. Although mild steel corrosion resistance is poor in aggressive environments, it is usually the most cost effective option with the use of organic corrosion inhibitors. Commercial corrosion inhibitors consist of at least one of the following surfactants: fatty acids, amines, fatty amines/diamines, fatty amido/amines or imidazolines, quaternary amines, other amine derivates, and oxygen, sulphur or phosphorous containing compounds [4].

It is generally accepted that organic molecules inhibit corrosion via adsorption at the metal-solution interface [5, 6]. Two primary mechanism of adsorption are associated with organic compounds: act by blocking the reaction sites or generating a physical barrier to reduce the diffusion of corrosive species to the metal surface. The mode of adsorption is dependent on the following factors: chemical and electronic structure of the molecule, inhibitor concentration, solution chemistry, nature and surface charge of the metal surface, electrochemical potential at the interface and the temperature of the corrosion reaction.

Temperature has a great effect on the rate of metal corrosion [7] and its variation is a very useful tool for studying and clarifying the adsorption mechanism of an inhibitor. It is well known that the effect of temperature is highly complex but it provides the

possibility of calculating the thermodynamic adsorption and kinetic corrosion parameters, which help in determining the type of adsorption of the studied inhibitor.

Despite significant progress has been achieved in understanding the mechanism of CO_2 corrosion in the oil and gas industry, the kinetics of the inhibition process necessary to quantify formulations for providing a desirable protection remains incomplete [3]. So, a better understanding of the inhibition mechanism and adsorption behaviour of imidazoline amide precursors is very important.

A detailed understanding of the mechanism of adsorption for corrosion inhibitors requires the characterization of corrosion inhibitor films by using surface analytical techniques such as Raman spectroscopy, X-ray photoelectron spectroscopy (XPS), Fourier transform infrared (FTIR) spectroscopy, etc. [4]. Electrochemical Impedance Spectroscopy (EIS) has proved to be a powerful technique to study corrosion processes and inhibitor performance in various concentrations and different temperatures. It can provide the information on corrosion and protection mechanism, especially when an adsorbed film or an organic coating is present [1, 8]. In addition, polarization methods were employed to evaluate corrosion rate and inhibition efficiency of the organic inhibitor at different temperatures. Recently, we have studied the corrosion behaviour of mild steel in CO_2-saturated 5% NaCl solution with N-[2-[(2-aminoethyl) amino] ethyl]-9-octadecenamide as corrosion inhibitor at 25 ºC [9]. The aim of this work is to continue the systematic study of this organic inhibitor, studying the temperature effect, thermodynamic of adsorption and activation energies of this amphiphilic amido-amine precursor in order to go forward to clarify how this inhibitor works in CO_2 media.

2. Experimental

2.1. Materials and medium

A mild steel SAE/AISI grade 1018 (Metal Samples) was used as working electrode. It was machined into 7 mm diameter bar, cut and mounted with epoxy resin in a disc electrode holder with an exposed area of 38 mm^2. Electrical contact between the sample and holder was obtained with silver loaded epoxy resin.

For the electrochemical tests, surfaces were abraded with 600-grit SiC paper, washed with distilled water and rinsed with ethanol. Experiments were conducted at atmospheric pressure and under low speed magnetic stirring. Three-electrode jacketed test cells with a working volume of 0.5 dm^3 and a concentric Pt ring as counter electrode were employed. A saturated calomel electrode (SCE) was chosen as reference. Testing solution was deaerated by purging CO_2 (99.95%) for 2 h prior to the experiments. The oxygen concentration of the solution was measured with a Fibox 3-trace v6 (PreSens GmbH) instrument with an accuracy of 1 μmol dm^{-3}, and it was kept below 40 μmol dm^{-3} during the experiments. Test solution was 5 wt% NaCl (analytical-reagent grade) saturated with deoxygenated CO_2. A positive pressure of deoxygenated CO_2 was maintained throughout the experiments to avoid air ingress. The pH was adjusted to 6 adding 0.01–0.015 dm^3 of deoxygenated 1.0 mol dm^{-3} $NaHCO_3$. After reaching the open circuit potential (2 h), potentiodynamic polarization and EIS measurements were carried out at temperatures of 25±1, 30±1, 35±1, 40±1 and 45±1 ºC in the absence and presence of various concentrations of the inhibitor. The inhibitor used in this study was N-[2-[(2-aminoethyl) amino] ethyl]-9-octadecenamide (AAOA) whose molecular formula is shown in Fig. 1. AAOA was synthesized from oleic acid and diethylenetriamine according to reference [9]. A stock solution was prepared by dissolving AAOA in isopropanol to 625 μmol dm^{-3}. The inhibitor was used in a concentration range of 0.68 to 55 μmol dm^{-3}.

Figure 1

The inhibitor was added at the beginning of the experiments and the formation of the inhibitor film was evaluated after 2 h of immersion, the time necessary to reach a quasi-stationary value for the open circuit potential (E_{corr}). The samples were kept at E_{corr} during their exposure to the corrosive medium.

2.2. Surface tension measurements

The surface tension (γ) was measured at 25 ºC by using a du Noüy tensiometer for various concentrations of the synthesized inhibitor. Solutions were prepared from the stock solution in isopropanol. The inhibitor was used in a concentration range of 3 to 35 μmol dm^{-3}.

2.3. Electrochemical measurements

A Voltalab PGZ 402 unit was used for electrochemical measurements. The linear polarization method was used for the determination of the polarization resistance (R_p) by polarizing the working electrode ±0.010 V vs. E_{corr} with a sweep rate of 10^{-4} V s^{-1}. The slope of the tangent at the origin provided the value of R_p. EIS was measured at the E_{corr} using an applied potential of ±0.01 V rms with a frequency range of 100000–0.01 Hz. The corrosion potential was also monitored before and after direct and alternate current (DC and AC) measurements.

Potentiodynamic polarization curves were drawn at the end of the experiments, with a sweep rate of 10^{-3} V s^{-1}. The scanning range was from E_{corr} to -0.45 V(SCE) for cathodic curves and from E_{corr} to 0.45 V(SCE) for anodic ones. The electrochemical

data were analyzed using the VoltaMaster 4 and Zview 2 software. At least four replicas were tested for each experimental condition. In order to characterize the surface attack, optical observation of the samples surface was done at the end of the experiments using an Olympus MG optical microscope.

The inhibition efficiency (η_i) was calculated as follows:

$$\eta_i = \left(\frac{R_p^{inh} - R_p^{0}}{R_p^{inh}} \right) 100 \quad (1)$$

where R_p^0 and R_p^{inh} are the uninhibited and inhibited polarization resistant, respectively [10, 11].

The corrosion current density (j_{corr}) was calculated applying the Stearn Geary equation ($B=0.022\ V$) [12]. For each condition, corrosion rate (C_R) was calculated using the Faraday law and the iron density. All the recorded j_{corr} values (expressed in µA cm^{-2}) were converted into the C_R in µm y^{-1} (micrometre per year, the penetration rate of corrosion through a metal) using the expression:

$$C_R = 3.27\, j_{corr} (M/nd) \quad (2)$$

where M is the atomic weight of Fe (55.85 g mol^{-1}), n the number of electrons transferred in the corrosion reaction (n=2) and d the iron density (7.88 g cm^{-3}) [7, 12].

The inhibition efficiencies of the studied inhibitor were also calculated from EIS results at different temperatures using the following equation:

$$\eta_i = \left(\frac{R_{ct}^{inh} - R_{ct}^{0}}{R_{ct}^{inh}} \right) 100 \quad (3)$$

where R_{ct}^{inh} and R_{ct}^{0} are the charge transfer resistance for solutions with and without inhibitor, respectively [1, 3].

3. Results and discussion

3.1. Adsorption isotherm

Classical adsorption isotherms have been used extensively in the study of adsorption of organic substances onto steel electrodes. It is widely acknowledged that they provide useful insights into the mechanism of corrosion inhibition [13]. A determination of the type of adsorption isotherm itself provides information on the adsorption process such as surface coverage, adsorption equilibrium constant and information on the interaction between the organic compound and electrode surface [1].

The adsorption of an organic inhibitor on the metal-solution interface causes the gradual replacement of water molecules originally adsorbed on the electrode surface, $H_2O_{(ads)}$, by the organic molecules in the aqueous solution, $Org_{(sol)}$. This process is represented as:

$$Org_{(sol)} + xH_2O_{(ads)} \rightarrow Org_{(ads)} + xH_2O_{(sol)} \quad (4)$$

where $Org_{(sol)}$ and $Org_{(ads)}$ are the organic molecules in the aqueous solution and the adsorbed molecules on the metallic surface, respectively, and x is the size ratio representing the number of water molecules replaced by one molecule of organic adsorbate [14].

Assuming that the steel electrode corrodes uniformly, the corrosion rate in the absence of inhibitor is representative of the total number of corroding sites. Also, the corrosion rate in the presence of low concentrations of the inhibitor is representative of the number of available corroding sites remaining after blockage of some sites due to inhibitor adsorption [13]. The melding of these assumptions enables a derivation for the fractional surface coverage (θ):

$$\theta = \frac{R_p^{inh} - R_p^{0}}{R_p^{inh}} \quad (5)$$

Table 1 shows R_p results from the lineal polarization method for mild steel electrodes in presence of various concentrations of inhibitor, C, at different temperatures after 2 h of immersion. In the range of temperature studied, the best correlation between the experimental results and isotherm functions was obtained using Frumkin adsorption isotherm [15]:

$$K_{ads}C = \frac{\theta}{1-\theta} e^{-2a\theta} \quad (6)$$

where K_{ads} is the adsorption equilibrium constant, C is the molar concentration of the inhibitor in the electrolyte and a is the molecular interaction constant ($a > 0$ indicates lateral attraction interactions between adsorbed inhibitor molecules, and $a < 0$ indicates lateral repulsion interactions between adsorbed inhibitor molecules). A plot of $\ln[\theta/C(1-\theta)]$ vs θ gives a straight line, as shown in Fig. 2.

Table 1

Figure 2

The obtained values of K_{ads} and a are given in Table 2. It can be observed that K_{ads} values decrease with the increasing temperature. This fact could indicate that the inhibitor AAOA is physically adsorbed on the metal surface [16]. In physical adsorption, the forces of attraction between the molecules of the adsorbate and the adsorbent are weak (van der Waals interactions). In contrast, in chemisorption, the forces of attraction between the adsorbate and the adsorbent are very strong. The molecules of adsorbate form chemical bonds with the molecules or atoms of the adsorbent present in the surface, involving charge sharing or charge transfer from the inhibitor molecules to the metal surface to form a coordinate type bond [17]. The high values of K_{ads} suggest that interaction between adsorbed molecules and the metal

surface is strong, indicating that the inhibitor molecules are not easily removable from the surface by the solvent molecules. Taking this into consideration, a strong adsorption bond of chemisorptive nature could be implicated. The obtained values of *a* are in the range of 0.46 to 1.40 from the lowest to the highest temperature studied, respectively. The parameter *a* is an average of the total attraction and repulsion forces between the adsorbed molecules. The positive sign of this constant implies the existence of attraction forces among adsorbed inhibitor molecules. A higher interaction constant is related to higher attractive lateral interactions between the adsorbed molecules. Durnie et al. [13] propose that this constant is dependent on the charge at the hydrophilic head group as well as steric factors.

Table 2

The thermodynamic of adsorption can provide valuable clues about the mechanism of corrosion inhibition [13, 17]. The adsorption equilibrium constant K_{ads} is related to the standard free energy of adsorption, ΔG_{ads}^{0} by the equation:

$$K_{ads} = \frac{1}{55.5} \exp \frac{(-\Delta G_{ads}^{0})}{RT} \quad (7)$$

where *55.5* is the molar concentration of water in solution and *R* and *T* have the usual meaning [17].

The calculated values of ΔG_{ads}^{0} are ranging between -41.9 and -41.1 kJ mol^{-1} (Table 2). These results indicate that the adsorption mechanism of AAOA on mild steel in CO_2 saturated solution is typical chemisorption at the studied temperatures. Generally, absolute values of ΔG_{ads}^{0} of the order of 20 kJ mol^{-1} indicate physisorption while those of the order of 40 kJ mol^{-1} or higher are associated with chemisorption [10, 18, 19]. The high and negative values obtained for ΔG_{ads}^{0} indicate that the adsorption process takes place spontaneously by strong interactions between the inhibitor and the steel surface, as was suggested by the obtained values of K_{ads}. Thermodynamically, ΔG_{ads}^{0} is related

to the enthalpy and entropy of adsorption process, ΔH_{ads}^{0} and ΔS_{ads}^{0}, respectively, by the equation:

$$\Delta G_{ads}^{0} = \Delta H_{ads}^{0} - T\Delta S_{ads}^{0} \quad (8)$$

Figure 3 shows the plot of ΔG_{ads}^{0} versus T which gives a straight line with an intercept of ΔH_{ads}^{0} and a slope of - ΔS_{ads}^{0} [18].

Figure 3

Adsorption is generally accompanied by release of energy, that is, most adsorption processes are exothermic in nature. An endothermic adsorption process ($\Delta H_{ads}^{0} > 0$) signifies unequivocally chemisorption, while an exothermic adsorption process ($\Delta H_{ads}^{0} < 0$) may involve either physisorption or chemisorption or a mixture of both the process [17, 18].

The obtained values of ΔH_{ads}^{0} and ΔS_{ads}^{0} are -54.2 kJ mol^{-1} and -41.2 J K^{-1} mol^{-1}, respectively. The ΔH_{ads}^{0} value in presence of the AAOA inhibitor is large and negative, indicating that the adsorption of the inhibitor molecules onto metal surface is an exothermic process. In an exothermic process, physisorption is distinguished from chemisorption by considering the absolute value of ΔH_{ads}^{0}. For the chemisorption process ΔH_{ads}^{0} approaches 100 kJ mol^{-1} while for the physisorption process, it is less than 40 kJ mol^{-1} [19, 20]. In the present study, the ΔH_{ads}^{0} value is larger than the expected physical adsorption but smaller than the one for chemical adsorption. This result suggests that the adsorption mechanism of AAOA on mild steel in CO_2 containing brines at the studied temperatures could involve both physisorption and chemisorption at concentrations less than or equal to 8.2 μmol dm^{-3}. Chemisorption of the AAOA molecules could occur due to the formation of links between the d orbital of iron atoms, involving the displacement of water molecules from the metal surface, and the lone sp_2 electron pairs present on the N and/or O atoms of the inhibitor. This was

confirmed by Polarization Modulation Infrared Reflection Absorption Spectroscopy (PM-IRRAS) experiments [9]. In these experiments, mild steel in presence of 8.2 μmol dm^{-3} of AAOA was rinsed with ethanol after the immersion period and AAOA molecules have not been removed from the surface.

The obtained negative value of ΔS_{ads}^{0} indicates a reduction of translational degrees of freedom. This means that an increase of order takes place in going from the free bulky AAOA molecules (inhibitor molecules are chaotic) to the more orderly inhibitor molecules onto the metal surface.

3.2. Surface tension measurements

It is well known that surfactants are characterized by critical micelle concentration (CMC). The CMC is the concentration where surfactants in solution change their initial molecular solvated state [21]. At this concentration, physical and chemical properties exhibit an abrupt variation. CMC values often exhibit a weak dependence on temperature. In order to obtain the CMC of AAOA, the surface tension (γ) of various concentrations of the inhibitor was measured at 25 ºC. The relation between γ and concentration is shown in Fig. 4. The intercept of the two lines indicates the CMC. It can be seen that the critical micelle concentration of AAOA is 15 μmol dm^{-3} approximately. It is known that highly dispersible, stable emulsion-like inhibitor solutions obtained at concentrations higher than CMC are more effective corrosion inhibitors than completely soluble inhibitor systems (below CMC).

Figure 4

3.3. Corrosion studies

3.3.1. DC electrochemical results

Temperature is a serious problem in corrosion because many changes occur on the inhibited metal surface such as rapid etching and desorption of inhibitor and the inhibitor itself may undergo decomposition and/or rearrangement [17]. Table 1 shows E_{corr}, C_R and inhibition efficiency results for mild steel in presence of various concentrations of inhibitor at different temperatures after 2 h of immersion. By optical microscopy it is observed that the whole surface of the samples is attacked by corrosion for all the experimental conditions, so no localized attack is experimentally observed.

As it can be seen from Table 1, corrosion rate increases with temperature in uninhibited solutions. This behaviour could be explained on the basis that increasing temperature accelerates all the other process involved in corrosion such as electrochemical reactions, chemical reactions and transfer process of reactive species to the metal surface [22]. In the presence of the inhibitor, corrosion rates are always much lower than those without inhibitor. These results indicate that the inhibitor is efficient at the range of temperature studied. For concentrations of the inhibitor less than or equal to 2.7 μmol dm^{-3}, the inhibition efficiency decreases by increasing the temperature from 25 to 45 ºC. This behaviour is characteristic of a physisorption mechanism because the strength of the interaction of inhibitor molecules with the metal surface decreases as temperature increases [23].

When concentrations of AAOA higher than 8.2 μmol dm^{-3} are added to the corrosive medium, this inhibitor proves to be highly efficient at all the studied temperatures. Moreover, it should be noted that at 8.2 μmol dm^{-3}, inhibition efficiency increases as temperature increases. At concentrations higher than 8.2 μmol dm^{-3}, the inhibition

efficiency remains high and almost constant with the increase of temperature. Such behaviour is often described in the literature for organic inhibitors at high concentrations. These results could indicate the formation of an inhibitor film on mild steel surface in which lateral interactions between AAOA molecules become important.

The corrosion behaviour of mild steel exposed to CO_2 containing brines without and with various concentrations of AAOA was also studied by potentiodynamic polarization curves in the temperature range of 25-45 ºC. Some of the polarization curves are given in Figure 5. From the analysis of this figure, it can be seen that there is a clear acceleration of both the anodic and cathodic reactions with the increase in temperature in uninhibited and inhibited solutions. Similar results have been reported previously in CO_2 containing brines [1, 3]. Moreover, there is not a significant change in Tafel slopes of the two branches of the polarization curves as temperature increases. The cathodic shift in E_{corr} values is in agreement with the acceleration of the dissolution of iron at higher temperatures.

As previously reported for 25 ºC [9], a great change in Tafel slopes is observed jointly with a more significant decrease of anodic currents in comparison with cathodic ones at concentrations of inhibitor higher than 8.2 μmol dm^{-3}. It might be explained by micellation above critical micelle concentration where maximum efficiencies are obtained [24]. At or above this CMC, the inhibitor molecules in the solution would form a surfactant bi-layer (admicelle) on mild steel surface [25]. At the conditions analyzed in the present study, this behaviour would start for concentrations of the inhibitor higher than 13.6 μmol dm^{-3}.

The anodic shift in E_{corr} is in agreement with the preferential inhibition of the anodic reaction which could be related to the formation of a protective film [25]. Polarization

curves shows that the studied compound is an inhibitor of the mixed type with the predominant influence on the anode process.

For every studied temperature, a sudden change in the slope of the anodic curve and an abrupt increase of the current can be observed at certain potential (Fig. 5b). The potential at which an abrupt increase of current density occurs when polarization potential reaches a relatively positive value is usually defined as the desorption potential, E_{des} [26, 27]. The curves in Figure 5b indicate that E_{des} decreases with increasing temperature, indicating that desorption of the inhibitor molecules from mild steel surface is favoured at higher temperatures.

Figure 5

Potentiodynamic curves obtained for mild steel electrode in CO_2 saturated solution show no Tafel dependence in anode region so corrosion current is determined graphically by extrapolation from the cathodic polarization curves. The polarization parameters are shown in Table 3.

Table 3

It can be seen from Table 3 that the current density and then the corrosion rate increase with temperature in both uninhibited and inhibited solutions. These results are in accordance with those calculated from linear polarization measurements (Table 1).

3.3.2. AC electrochemical results

Figure 6 shows Nyquist and Bode plots of mild steel after 2 h of immersion in CO_2 saturated solutions without inhibitor at different temperatures. The effect of the addition of AAOA inhibitor is exemplified in Figure 7 for a concentration of 27.2 μmol dm^{-3}.

Figure 6

Figure 7

As it can be seen in Figs. 6 and 7 (a), the Nyquist plots have the form of depressed semicircles with the centre under the real axis. The depressed semicircle form is characteristic of a dispersion in frequency and has been attributed to different physical phenomena such as roughness and inhomogeneities of solid surfaces during corrosion [28]. It is observed that increasing the temperature decreases the radius of the semicircle, which indicates higher corrosion rates. The continuous decrease in the diameter of the Nyquist semicircle and in the impedance module with temperature is in agreement with the former DC measurements. In the Bode plot of Fig. 6b, it can be seen that the value of the maximum phase angle of the time constant at a frequency about 20 Hz decreases due to the increase of the temperature solution. This time constant can be attributed to the double layer capacitance so this behaviour could be related to the fact that the product blocks less portion of the active surface area of the mild steel electrode.

Electrical equivalent circuits are generally used to model the electrochemical behaviour of real systems. When modelling corrosion problems, ideal capacitors are frequently replaced by Constant Phase Elements (CPE) representing leaky or non-ideal capacitors with a view to compensating for non-homogeneity in the system [29]. The impedance of a CPE is described by the following expression:

$$Z_{CPE} = Y^{-1}(i\omega)^{-n} \qquad (9)$$

where Y is proportional to the capacitance of the corroding system [30], i is $\sqrt{-1}$, ω is $2\pi f$, and n represents a phase shift [6, 29].

The corresponding electrical equivalent circuit model for the mild steel in uninhibited solution at different temperatures is given in Fig. 8a, where R_s is the electrolyte resistance, R_{ct} is the charge transfer resistance, Y_{CPEdl} is proportional to the double layer capacitance C_{dl}, and n_{CPEdl} is the constant phase element exponent. The experimental

results for concentrations of the inhibitor less than or equal to 2.7 μmol dm^{-3} were modelled by a equivalent circuit representing a partial surface covered by the organic molecules (Fig. 8b), where R_1 is the resistance of the inhibitor film pores, Y_{CPE1} is proportional to the capacitance of the film C_F, and n_{CPE1} is the constant phase element exponent [1].

Figure 8

For samples corroded 2 h with 8.2 μmol dm^{-3} of the corrosion inhibitor, the analysis of the impedance spectra was done using an equivalent circuit given in Fig. 8c. This model represents the formation of a porous monolayer on mild steel surface. In this electrical circuit Z_W is a finite length Warburg impedance element that represents the diffusion of reactive species. This impedance element is calculated by the equation [29]:

$$Z_W = R_W (T_W i\omega)^{-n} \tanh(T_W i\omega)^n \quad (10)$$

where R_W is the diffusion resistance, T_W represents the relation l_e^2/D_e, being D_e the effective diffusion coefficient of the reactive species and l_e the effective diffusion thickness. The exponent n is equal to 0.5.

The equivalent circuit used to model impedance data for inhibitor concentrations greater than or equal to 13.6 μmol dm^{-3} is given in Fig. 8d. At this range of concentration of the organic inhibitor, there is a change in its behaviour which was modelled considering a porous bi-layer and diffusion processes within pores in the film. These results are in accordance with the development of admicelles at higher concentrations than CMC. In this equivalent circuit Z_{CPE2} and R_2, and Z_{CPE1} and R_1 are related to the non-ideal capacitance and to the pore resistances of the outer and inner layer of the inhibitor film, respectively.

As a representative example, the fitting results for the impedance spectra corresponding to 25, 35 and 45 ºC in absence and presence of the AAOA inhibitor are shown en Fig. 6

and 7, respectively. In all cases the fitted data have an average error lower than 5%. The values of impedance parameters obtained by fitting the impedance data are listed in Table 4 and 5. In all cases the fitted data have an average error lower than 5%. As can be seen in Table 4, the R_{ct} values decrease with the increase of temperature at each concentration studied, resulting in a decrease in inhibition efficiency. These results show the same trend as those obtained by the linear polarization resistance method and polarization curves. On the other hand, Y_{CPEdl} values increase with increasing temperature which means that less inhibitor molecules are adsorbed to mild steel surface [27]. Generally, the values of n_{CPEdl} decrease with increasing temperature. This fact may be described by the roughening of the mild steel surface which results from enhanced corrosion [31].

Table 4

The resistances of the inner (R_1) and the outer layer (R_2) decrease with temperature. This suggests that the number of pores per unit area and/or the pores size penetrated by the electrolyte are higher. Moreover, R_1 is always higher than R_2 at each temperature and concentration studied. This could be related to an inner layer with a higher molecular density as has been proposed previously by other authors [32, 33]. On the other hand, Table 5 shows lower values of T_{W1} and T_{W2} as temperature increases. This phenomenon suggests that it is easier for aggressive ions to diffuse through pores within the inner or outer layer at higher temperatures which is reasonable considering that the diffusion coefficient increases with temperature. Then the bi-layer inhibitor film (admicelle) should have pores with lower effective diffusion thickness.

Table 5

Considering the effect of temperature on the behaviour of the AAOA corrosion inhibitor, EIS results together with those obtained from linear polarization method and

polarization curves, reveal a change in the nature of the adsorption mode of the inhibitor studied: the inhibitor AAOA could primarily be physically adsorbed at concentrations lower than 2.7 μmol dm^{-3}, while chemisorption could be favoured as concentration increases [34]. These results are in accordance with those obtained from the adsorption isotherms.

From a practical point of view, in CO_2 containing brines the recommended concentration of an inhibitor should be one that assures a minimum efficiency of 95%. It can be seen that in the selected experimental conditions this minimum concentration would be 13.6 μmol dm^{-3} at any temperature analyzed. It is important to note that the behaviour of the AAOA inhibitor at 13.6 μmol dm^{-3} is not dependent of temperature. Considering the experimental conditions of the present study, a concentration of 13.6 μmol dm^{-3} could be chosen to obtain very high corrosion efficiencies up to 40 ºC.

3.3.2. Corrosion activation parameters

The activation parameters for the corrosion process can be calculated from Arrhenius-type plot using the following equation:

$$j_{corr} = k \exp\left(-\frac{E_{act}}{RT}\right) \quad (11)$$

where j_{corr} is the corrosion current density obtained from the polarization resistant method, k is an Arrhenius pre-exponential factor, E_{act} is the apparent activation energy of the corrosion process and R and T have the usual meaning [17]. Some relevant information about the adsorption mechanism of the inhibitor can be obtained by comparing E_{act}, both in the absence and presence of the corrosion inhibitor. The corresponding Arrhenius plots are shown in Fig. 9. In this figure, the lineal fitting

results corresponding to 0, 0.7, 1.4, 2.7, 8.2, 13.6, 27.2 and 54.4 μmol dm^{-3} of inhibitor concentration are shown as representative examples.

Figure 9

Values of the apparent activation energy of corrosion for carbon steel in CO_2 saturated solution in the absence and presence of different concentrations of AAOA were determined from the slope of ln j_{corr} versus $1/T$ plots and are given in Table 6.

Table 6

The value of the activation energy of the corrosion process in absence of the inhibitor in CO_2 containing brines is 33.4 kJ mol^{-1}, which is close to the value cited by Okafor et al. [3]. Moreover, it can be seen that for the range of AAOA inhibitor concentrations between 0.7 and 2.7 μmol dm^{-3}, E_{act} is lower in the absence than in the presence of inhibitor (42.6-45.1 kJ mol^{-1}). The increase in apparent activation energy in the presence of inhibitor compared to its absence jointly with a decrease in inhibition efficiency with rise in temperature is often ascribed in literature to the formation of an inhibitor film physically adsorbed [31, 35, 36]. For the adsorption of organic molecules on mild steel surface, the values of apparent activation energy are in the range of 30 to 50 kJ mol^{-1} [1]. These results are in accordance with those listed in Table 6 for concentrations of the AAOA inhibitor lower than 8.2 μmol dm^{-3}. The opposite dependence (lower apparent activation energy in an inhibited solution) is related to a chemisorptive bond between the inhibitor and the metal surface [31, 37]. In the present study, E_{act} value for the inhibited systems increases with inhibitor concentration until it reaches a maximum value at concentration of AAOA of 2.7 μmol dm^{-3} after which, a decrease in E_{act} value with further increase in inhibitor concentration is observed. The above results hint at a change of the adsorption behaviour with concentration of the studied inhibitor, as was previously explained in section 3.3.2. The most probable rationale for the above

observation could be the blocking of reaction sites of mild steel primarily by physisorption in the lower concentration range [9]. This is possible because the AAOA molecules have three nitrogen atoms with electron-pair donors that can accept a proton, leading the cationic forms. In this form, these species can interact with metal surface by attractive forces between the negatively charged metal and the positively charged inhibitor. In this range of concentration (0.7 to 2.7 μmol dm^{-3}), molecules can lay flat to the surface and can also be oriented perpendicularly. In the first orientation, hydrocarbon chains can also interact with iron through the π electrons of the double bond in the hydrocarbon chain.

When the inhibitor concentration increases, the anodic sites of metal surface could be also blocked by chemisorption of the electron rich amine or carbonilic moieties to the metal surface. This could be the case for concentrations of the inhibitor higher than 8.2 μmol dm^{-3} because there is almost no change in the apparent activation energy. Vracar et al [35] proposed that mixed adsorption could take place, which also agrees with the results presented in section 3.1. At 8.2 μmol dm^{-3}, molecules form a porous monolayer with strong lateral interactions, probably oriented vertically. The self-assembly of molecules is improved by the presence of the double bond in the hydrocarbon chain that may facilitate the interaction between molecules. At concentrations of the inhibitor higher than 8.2 μmol dm^{-3}, it can be seen from Table 6 that the E_{act} decreases with increasing concentration of AAOA. This is an indication of chemical adsorption of the inhibitor on mild steel surface [3, 17] and is in accordance with the high and temperature independent efficiencies (Table 1). At high inhibitor concentrations, the surface is saturated and a protective bi-layer is formed (see section 3.3.1 and 3.3.2). This is also in accordance with other authors suggestions [11, 33, 38]. The interaction of iron, a transition metal with a vacant, low-energy electron orbital and the loosely bound

electron, with N and O heteroatoms in the AAOA molecule support this proposition for the adsorption mechanism [17, 39].

4. Conclusions

Electrochemical methods are used to study the effect of temperature (25-45 ºC) on the surface coverage and inhibition performance of an amphiphilic amido-amine as a corrosion inhibitor for mild steel exposed to CO_2 saturated solution.

The study of the effect of temperature on the surface coverage shows that the adsorption of the AAOA corrosion inhibitor obeys a Frumkin adsorption isotherm where lateral attractive interactions between AAOA adsorbed molecules are compatible with a self-assembly film formation. The inhibitor AAOA is primarily physically adsorbed at concentrations lower than 2.7 μmol dm^{-3}, while chemisorption is favoured as concentration increases.

The inhibition efficiency of the AAOA depends on temperature and concentration. For the lower concentration range (less than or equal to 2.7 μmol dm^{-3}) the inhibition efficiency decreases with the increase in temperature, suggesting that physical adsorption primarily occurs, in agreement with the values of the adsorption equilibrium constant K_{ads}. For concentrations higher than or equal to 8.2 μmol dm^{-3}, the inhibition efficiency remains high and almost constant with the increase of temperature, suggesting that chemical adsorption mainly occurs.

The apparent activation energy of the corrosion process for the inhibited condition is higher respect to that in the uninhibited condition for the lower concentration range meanwhile the opposite happens for the higher concentrations. These results are in

agreement with a change in the adsorption mode for the range of concentrations and temperatures studied.

Acknowledgements

This work was supported by the Argentine Research Council for Science and Technology (CONICET) and by the University of Mar del Plata.

References

[1] G. Zhang, C. Chen, M. Lu, C. Chai, Y. Wu, Evaluation of inhibition efficiency of an imidazoline derivative in CO2-containing aqueous solution, Mater. Chem. Phys. 105 (2007) 331-340.

[2] R. De Marco, W. Durnie, A. Jefferson, B. Kinsella, A. Crawford, Persistence of carbon dioxide corrosion inhibitors, Corrosion 58 (2002) 354-363.

[3] P.C. Okafor, X. Liu, Y.G. Zheng, Corrosion inhibition of mild steel by ethylamino imidazoline derivative in CO2-saturated solution, Corros. Sci. 51 (2009) 761-768.

[4] W.H. Durnie, B.J. Kinsella, R. De Marco, A. Jefferson, A study of the adsorption properties of commercial carbon dioxide corrosion inhibitor formulations, J. Appl. Electrochem. 31 (2001) 1221-1226.

[5] O. Olivares-Xometl, N.V. Likhanova, M.A. Domínguez-Aguilar, E. Arce, H. Dorantes, P. Arellanes-Lozada, Synthesis and corrosion inhibition of [alpha]-amino acids alkylamides for mild steel in acidic environment, Mater. Chem. Phys. 110 (2008) 344-351.

[6] G. Quartarone, M. Battilana, L. Bonaldo, T. Tortato, Investigation of the inhibition effect of indole-3-carboxylic acid on the copper corrosion in 0.5 M H2SO4, Corros. Sci. 50 (2008) 3467-3474.

[7] M.A. Amin, M.A. Ahmed, H.A. Arida, T. Arslan, M. Saracoglu, F. Kandemirli, Monitoring corrosion and corrosion control of iron in HCl by non-ionic surfactants of the TRITON-X series - Part II. Temperature effect, activation energies and thermodynamics of adsorption, Corros. Sci. 53 (2011) 540-548.

[8] B. Wang, M. Du, J. Zhang, C.J. Gao, Electrochemical and surface analysis studies on corrosion inhibition of Q235 steel by imidazoline derivative against CO2 corrosion, Corros. Sci. 53 (2011) 353-361.

[9] M.P. Desimone, G. Grundmeier, G. Gordillo, S.N. Simison, Amphiphilic amido-amine as an effective corrosion inhibitor for mild steel exposed to CO2 saturated solution: Polarization, EIS and PM-IRRAS studies, Electrochim. Acta 56 (2011) 2990-2998.

[10] S. Ghareba, S. Omanovic, Interaction of 12-aminododecanoic acid with a carbon steel surface: Towards the development of green corrosion inhibitors, Corros. Sci. 52 (2010) 2104-2113.

[11] L.D. Paolinelli, T. Pérez, S.N. Simison, The incidence of chromium-rich corrosion products on the efficiency of an imidazoline-based inhibitor used for CO2 corrosion prevention, Mater. Chem. Phys. 126 (2011) 938-947.

[12] D.A. Jones, Principles and Prevention of Corrosion, Macmillan, 1991.

[13] W. Durnie, R. De Marco, A. Jefferson, B. Kinsella, Development of a structure-activity relationship for oil field corrosion inhibitors, J. Electrochem. Soc. 146 (1999) 1751-1756.

[14] J.O.M. Bochris, D.A.J. Swinkels, J. Electrochem. Soc. 111 (1964) 36.

[15] A. Popova, M. Christov, A. Vasilev, Inhibitive properties of quaternary ammonium bromides of N-containing heterocycles on acid mild steel corrosion. Part I: Gravimetric and voltammetric results, Corros. Sci. 49 (2007) 3276-3289.

[16] E.E. Oguzie, B.N. Okolue, E.E. Ebenso, G.N. Onuoha, A.I. Onuchukwu, Evaluation of the inhibitory effect of methylene blue dye on the corrosion of aluminium in hydrochloric acid, Mater. Chem. Phys. 87 (2004) 394-401.

[17] F. Bentiss, M. Lebrini, M. Lagrenee, Thermodynamic characterization of metal dissolution and inhibitor adsorption processes in mild steel/2,5-bis(n-thienyl)-1,3,4-thiadiazoles/hydrochloric acid system, Corros. Sci. 47 (2005) 2915-2931.

[18] H.H. Hassan, Inhibition of mild steel corrosion in hydrochloric acid solution by triazole derivatives: Part II: Time and temperature effects and thermodynamic treatments, Electrochim. Acta 53 (2007) 1722-1730.

[19] E.A. Noor, A.H. Al-Moubaraki, Thermodynamic study of metal corrosion and inhibitor adsorption processes in mild steel/1-methyl-4[4'(-X)-styryl pyridinium iodides/hydrochloric acid systems, Mater. Chem. Phys. 110 (2008) 145-154.

[20] L. Herrag, B. Hammouti, S. Elkadiri, A. Aouniti, C. Jama, H. Vezin, F. Bentiss, Adsorption properties and inhibition of mild steel corrosion in hydrochloric solution by some newly synthesized diamine derivatives: Experimental and theoretical investigations, Corros. Sci. 52 (2010) 3042-3051.

[21] R. Fuchs-Godec, The adsorption, CMC determination and corrosion inhibition of some N-alkyl quaternary ammonium salts on carbon steel surface in 2 M H2SO4, Colloid Surface A 280 (2006) 130-139.

[22] S. Nesic, Key issues related to modelling of internal corrosion of oil and gas pipelines - A review, Corros. Sci. 49 (2007) 4308-4338.

[23] M. Honarvar Nazari, S.R. Allahkaram, M.B. Kermani, The effects of temperature and pH on the characteristics of corrosion product in CO2 corrosion of grade X70 steel, Materials & Design 31 (2010) 3559-3563.

[24] I. Esih, T. Soric, Z. Pavlinic, Time dependence of inhibiting effect of amidoamines in CO2 saturated chloride solutions, Brit. Corros. J. 33 (1998) 309-314.

[25] V. Jovancicevic, S. Ramachandran, P. Prince, Inhibition of carbon dioxide corrosion of mild steel by imidazolines and their precursors, Corrosion 55 (1999) 449-455.

[26] X. Liu, P.C. Okafor, Y.G. Zheng, The inhibition of CO2 corrosion of N80 mild steel in single liquid phase and liquid/particle two-phase flow by aminoethyl imidazoline derivatives, Corros. Sci. 51 (2009) 744-751.

[27] X.Y. Zhang, F.P. Wang, Y.F. He, Y.L. Du, Study of the inhibition mechanism of imidazoline amide on CO2 corrosion of Armco iron, Corros. Sci. 43 (2001) 1417-1431.

[28] K. Jüttner, Electrochemical impedance spectroscopy (EIS) of corrosion processes on inhomogeneous surfaces, Electrochim. Acta 35 (1990) 1501-1508.

[29] ZPlot for Windows, Electrochemical Impedance Software Operating Manual, in, Scibner Associates Inc., Southern Pines, NC, 1998.

[30] C.H. Hsu, F. Mansfeld, Technical note: Concerning the conversion of the constant phase element parameter Y-0 into a capacitance, Corrosion 57 (2001) 747-748.

[31] A. Popova, E. Sokolova, S. Raicheva, M. Christov, AC and DC study of the temperature effect on mild steel corrosion in acid media in the presence of benzimidazole derivatives, Corros. Sci. 45 (2003) 33-58.

[32] Y.J. Tan, S. Bailey, B. Kinsella, The monitoring of the formation and destruction of corrosion inhibitor films using electrochemical noise analysis (ENA), Corros. Sci. 38 (1996) 1681-1695.

[33] L.D. Paolinelli, T. Pérez, S.N. Simison, The effect of pre-corrosion and steel microstructure on inhibitor performance in CO2 corrosion, Corros. Sci. 50 (2008) 2456-2464.

[34] E.S. Ivanov, Inhibitors for metal corrosion in acid media, Metallurgy, Moscow (1986).

[35] L.M. Vracar, D.M. Drazic, Adsorption and corrosion inhibitive properties of some organic molecules on iron electrode in sulfuric acid, Corros. Sci. 44 (2002) 1669-1680.

[36] A. Conde, J.J. de Damborenea, Electrochemical impedance spectroscopy for studying the degradation of enamel coatings, Corros. Sci. 44 (2002) 1555-1567.

[37] T. Szauer, A. Brandt, On the role of fatty acid in adsorption and corrosion inhibition of iron by amine--fatty acid salts in acidic solution, Electrochim. Acta 26 (1981) 1257-1260.

[38] M.M. Osman, R.A. El-Ghazawy, A.M. Al-Sabagh, Corrosion inhibitor of some surfactants derived from maleic-oleic acid adduct on mild steel in 1 M H2SO4, Mater. Chem. Phys. 80 (2003) 55-62.

[39] F.S. de Souza, A. Spinelli, Caffeic acid as a green corrosion inhibitor for mild steel, Corros. Sci. 51 (2009) 642-649.

Figure Captions

Fig. 1: N-[2-[(2-aminoethyl) amino] ethyl]-9-octadecenamide (AAOA).

Fig. 2: Curve fitting of the corrosion data for mild steel in CO_2 saturated solution in the presence of AAOA according to Frumkin isotherm model at different temperatures: a) 25 ºC, b) 30 ºC, c) 35 ºC, d) 40 ºC and e) 45 ºC.

Fig. 3: Variation of ΔG_{ads}^{0} vs. T on mild steel in CO_2-saturated 5% NaCl solution containing the AAOA inhibitor.

Fig. 4: Variation of the surface tension with concentration of AAOA inhibitor at 25 ºC.

Fig. 5: Polarization curves of mild steel exposed in CO_2-saturated 5% NaCl solution containing (a) 0 µmol dm^{-3}, and (b) 54.4 µmol dm^{-3} of AAOA inhibitor at: — 25 ºC, -■- 35 ºC and -Δ- 45 ºC.

Fig. 6: Nyquist (a) and Bode (b) plots of mild steel exposed in a CO_2-saturated 5% NaCl solution without inhibitor at different temperatures: -○- 25 ºC, -■- 35 ºC and -Δ- 45 ºC; ── fitting results.

Fig. 7: Nyquist (a) and Bode (b) plots of mild steel exposed in a CO_2-saturated 5% NaCl solution with 27.2 µmol dm^{-3} of AAOA at different temperatures: -○- 25 ºC, -■- 35 ºC and -Δ- 45 ºC; ── fitting results.

Fig. 8: Different equivalent circuits used for the modelling of the impedance data.

Fig. 9: Arrhenius plots for mild steel in CO_2-saturated 5% NaCl solution in absence and in presence of: (a) -■- 0 µmol dm^{-3}, -□- 0.7 µmol dm^{-3}, -▲- 1.4 µmol dm^{-3} and -∇- 2.7 µmol dm^{-3} of AAOA inhibitor; (b) -◁- 8.2 µmol dm^{-3}, -▼- 13.6 µmol dm^{-3}, -○- 27.2 µmol dm^{-3} and -●- 54.4 µmol dm^{-3} of AAOA inhibitor.

Figure 1

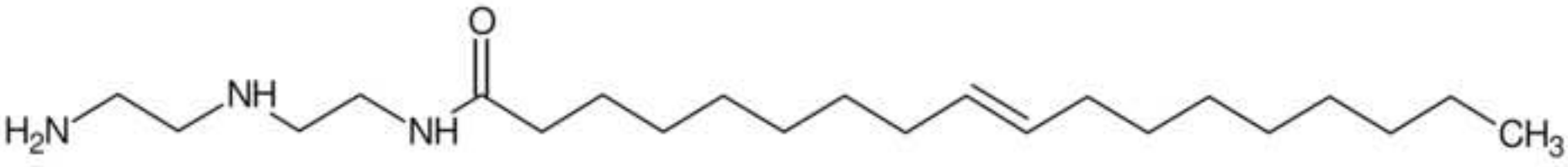

Figure 2

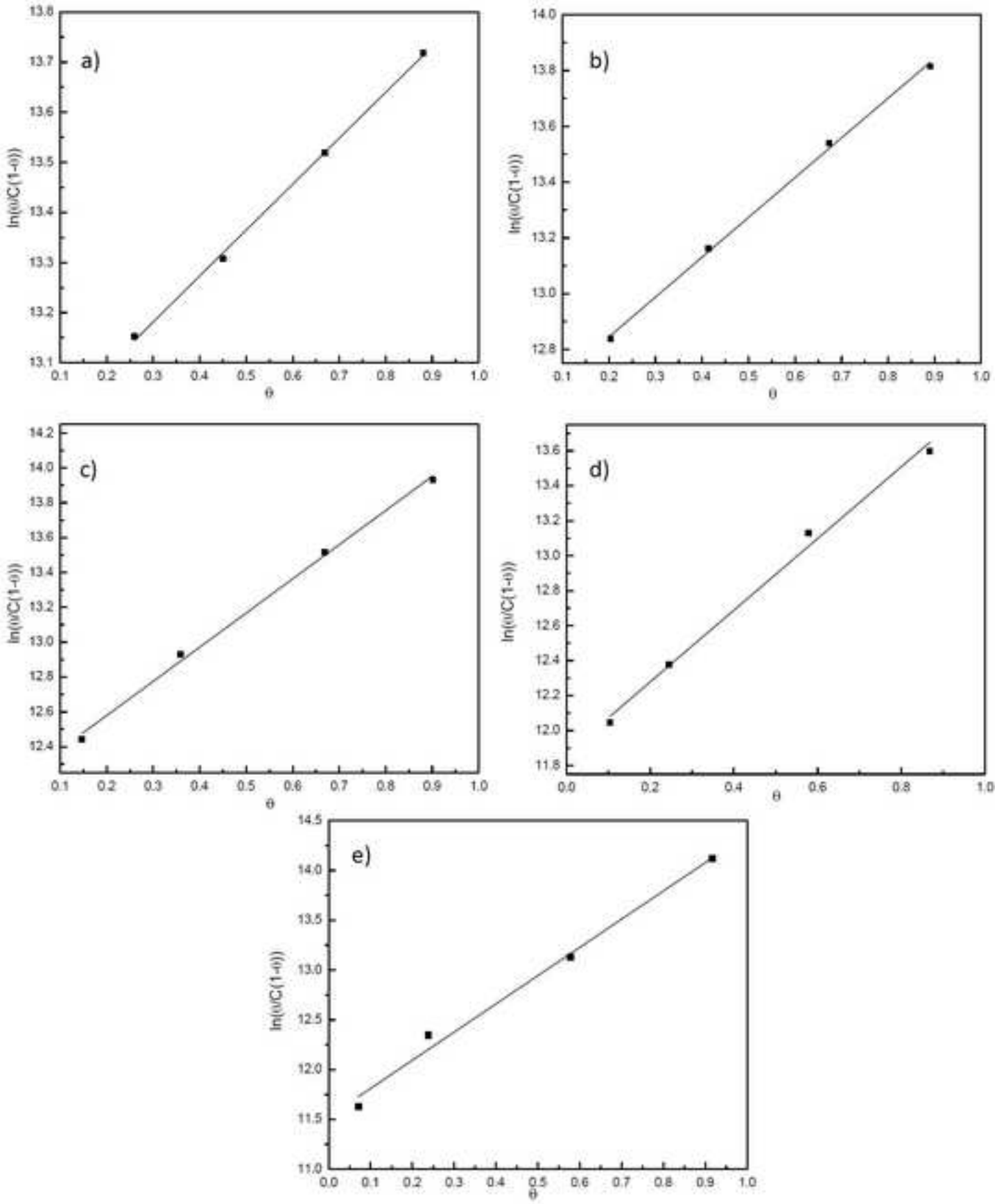

Figure 3

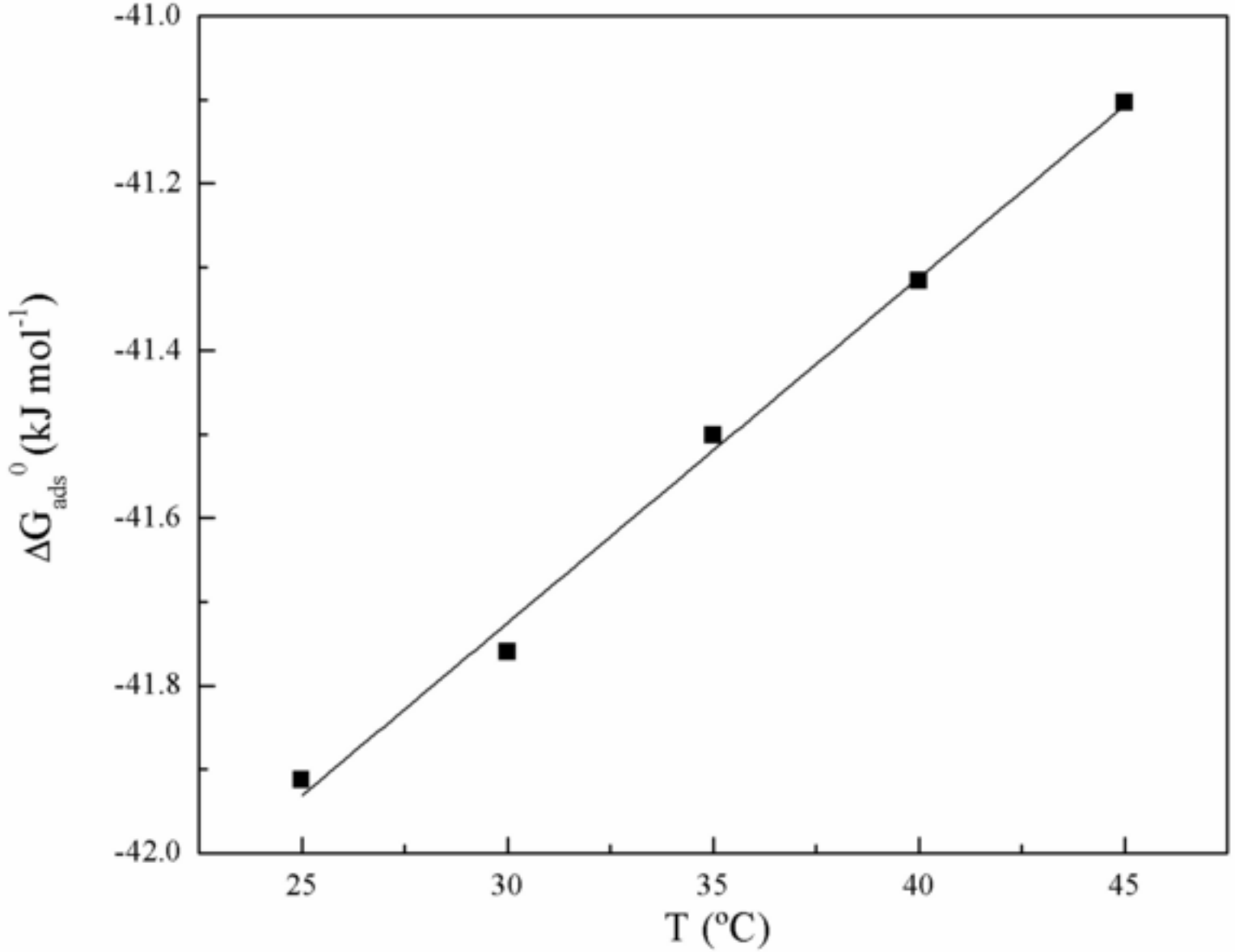

Figure 4

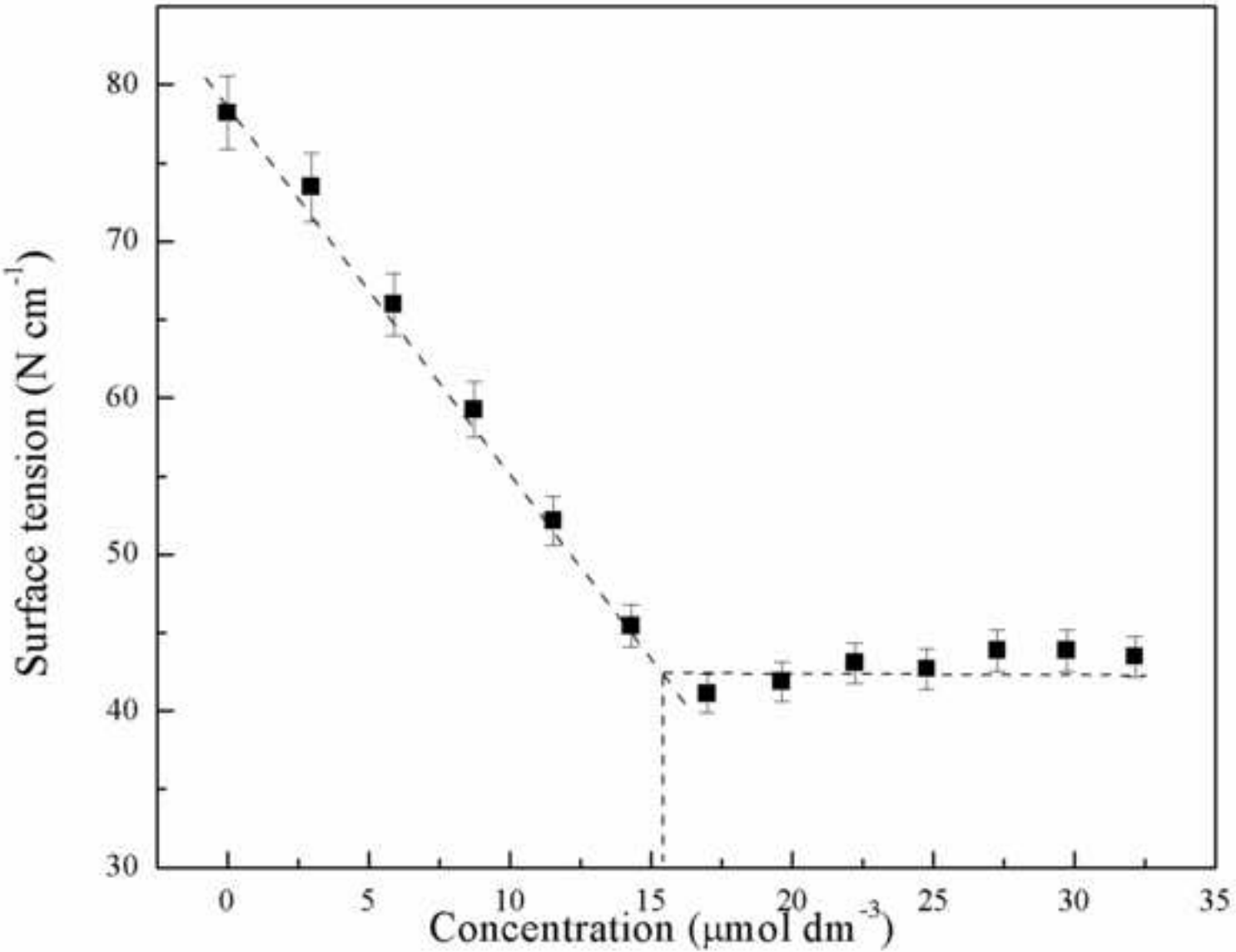

Figure 5

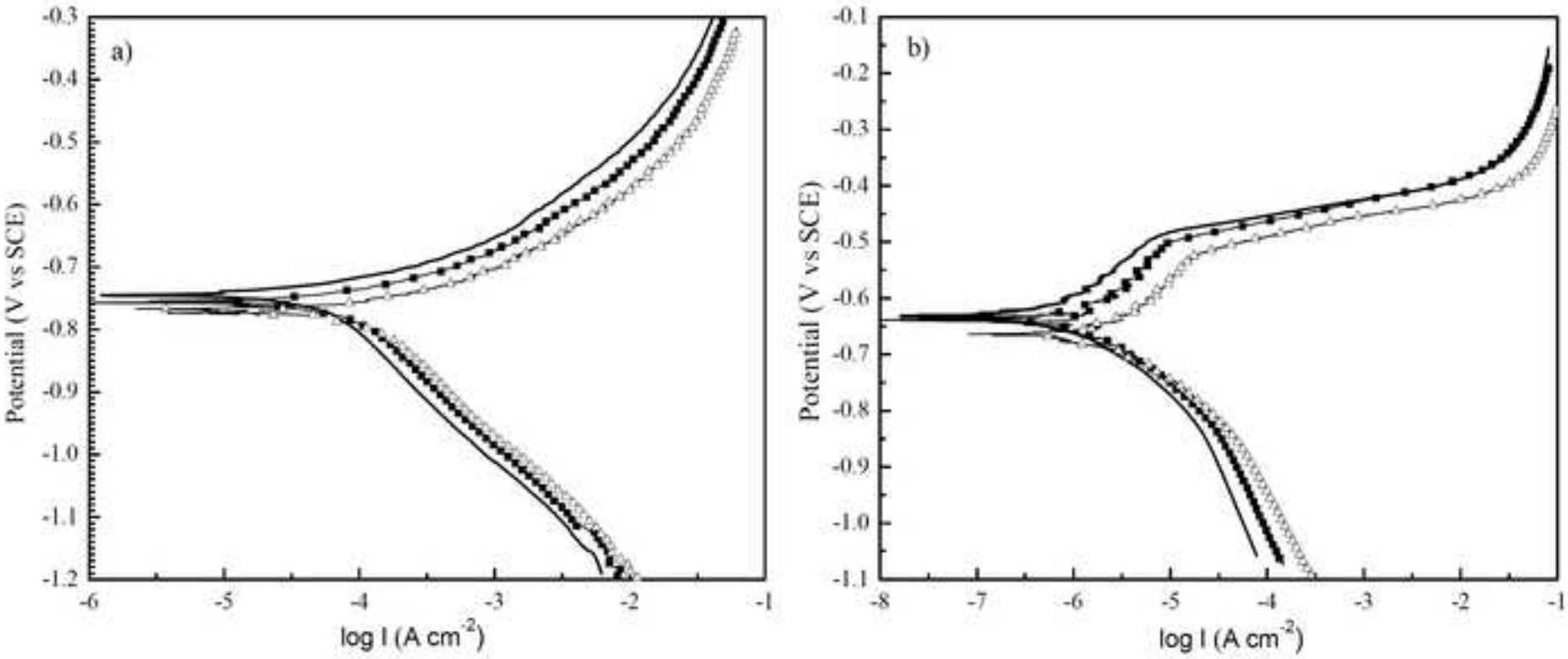

Figure 6

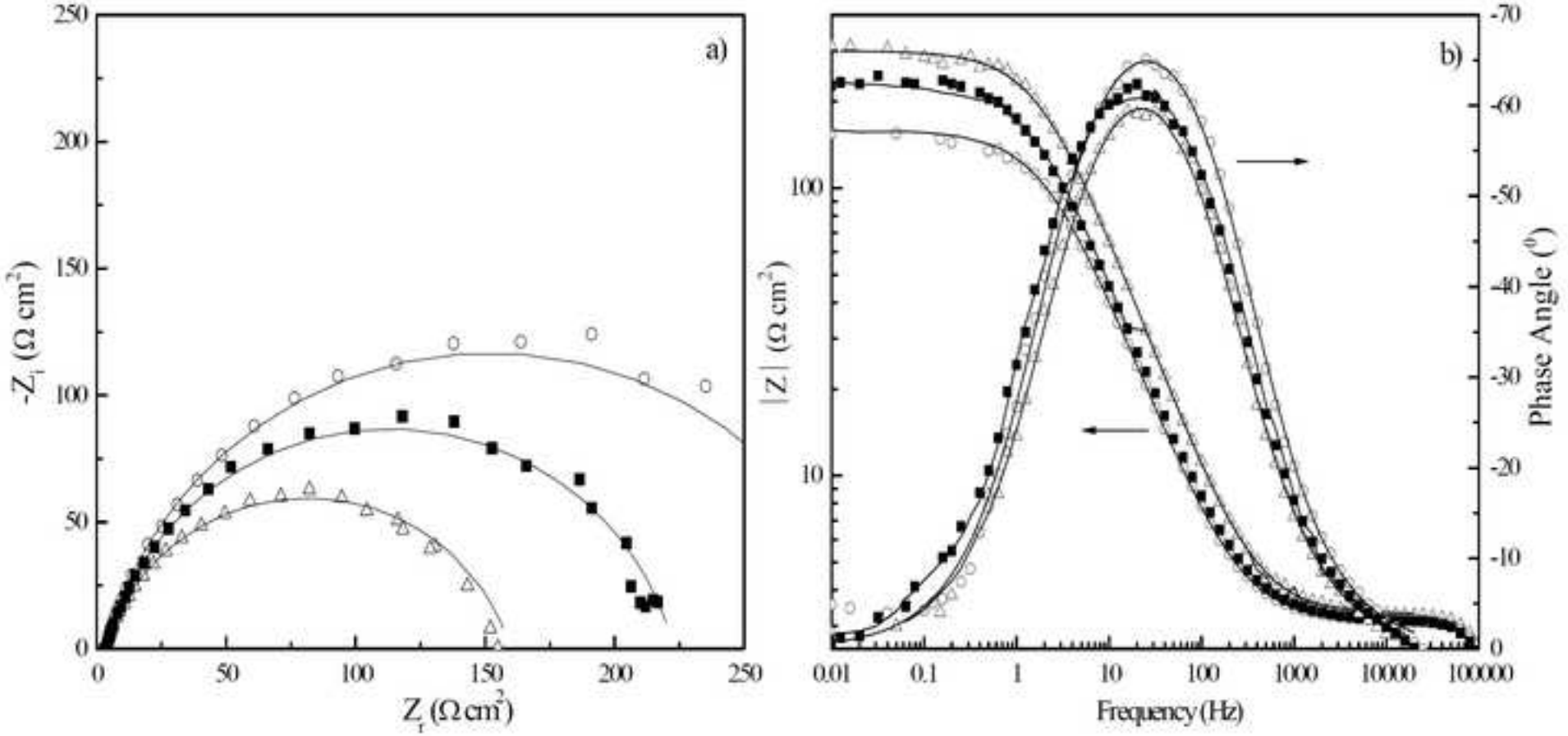

Figure 7

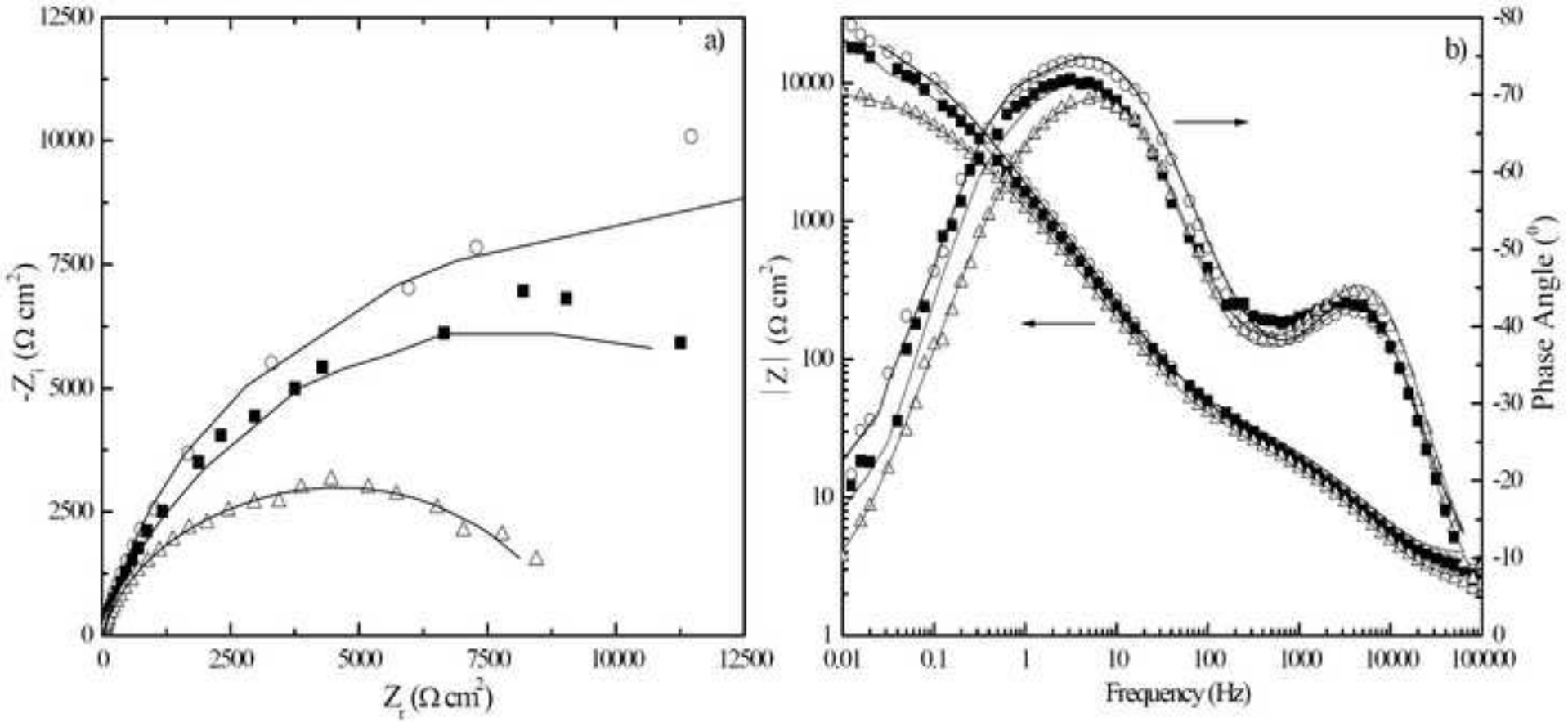

Figure 8

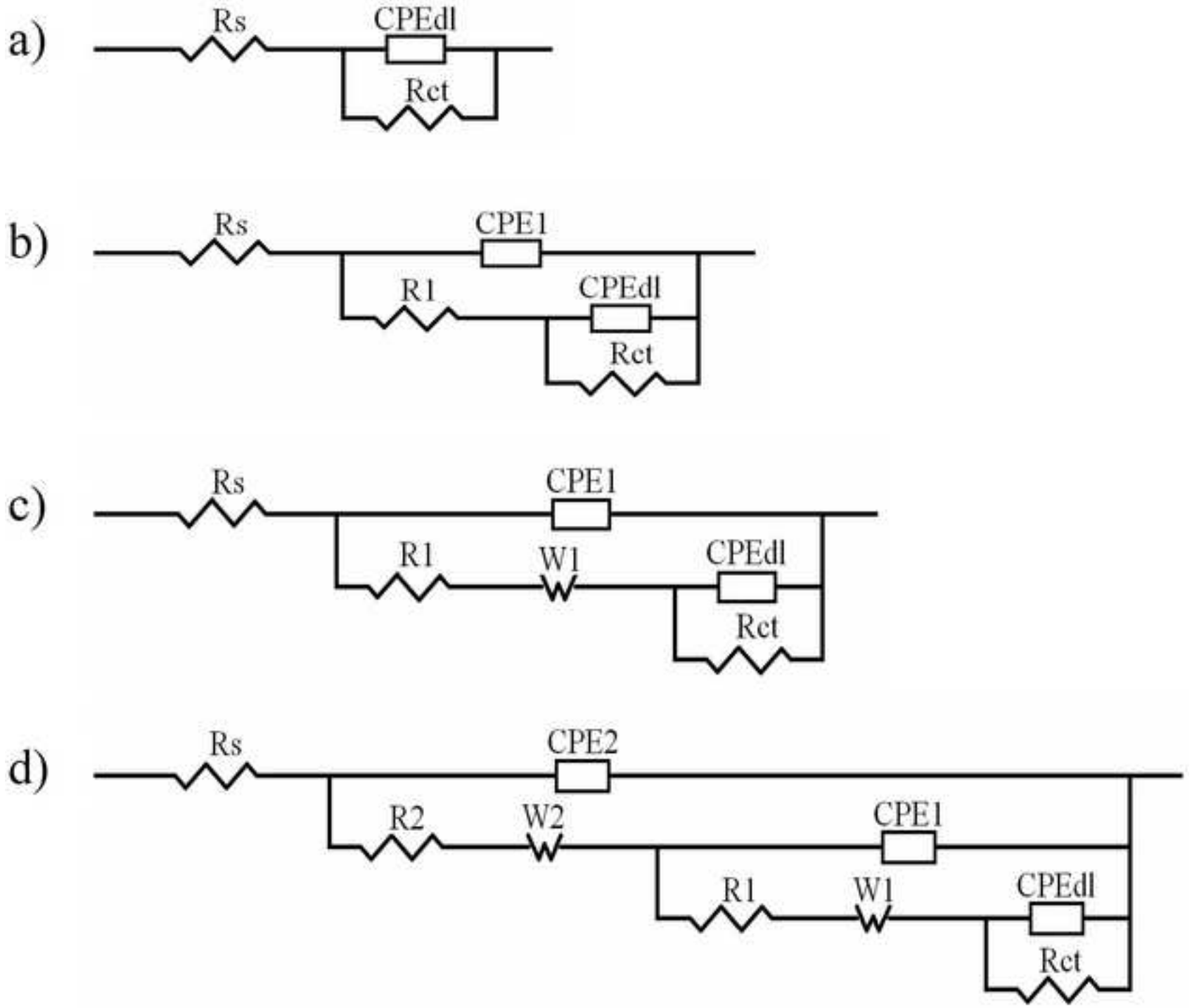

Figure 9

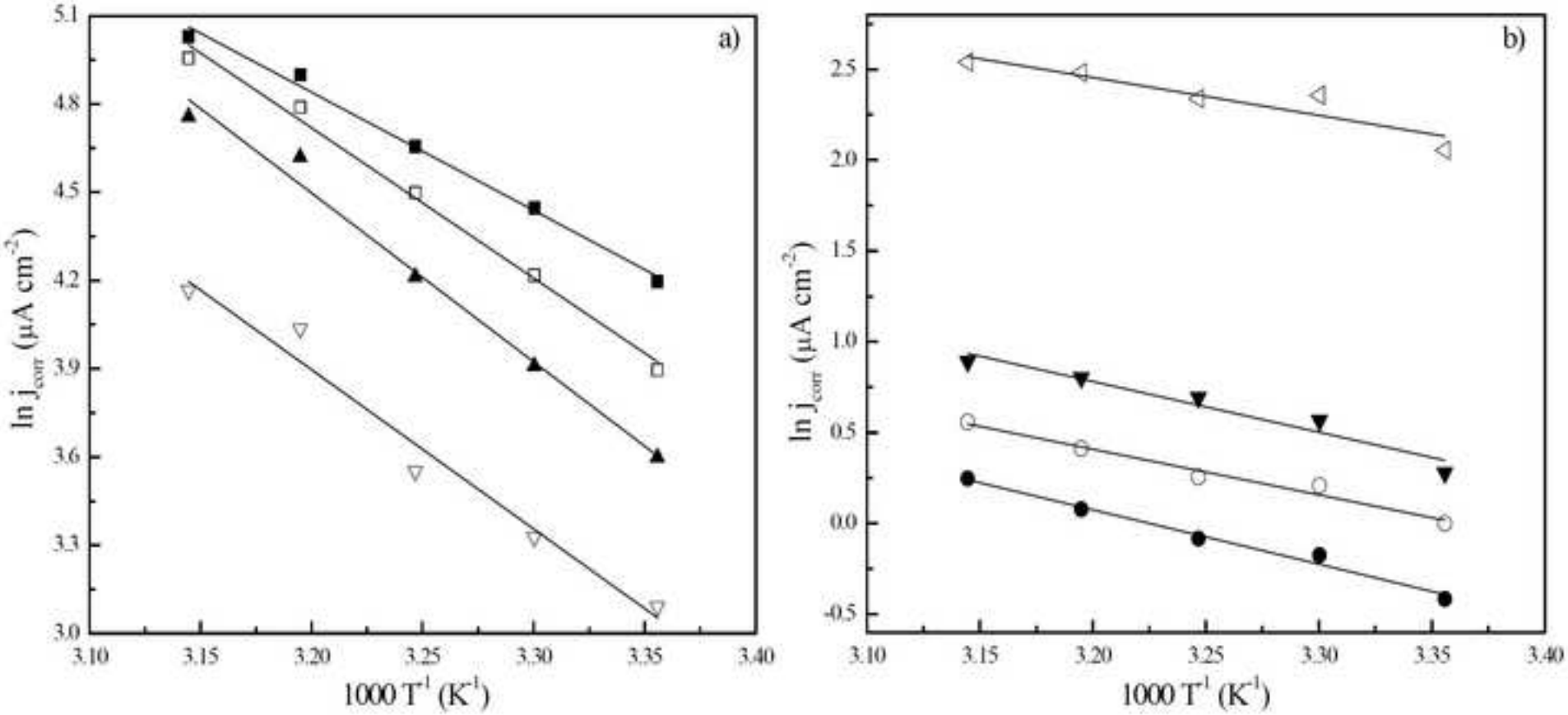

Table 1: Electrochemical measurements for mild steel in a CO_2 media containing various concentrations of the inhibitor for 2 h at different temperatures.

C (μmol dm^{-3})	Temperature (°C)	E_{corr} (mV vs SCE)	R_p (Ω cm^2)	C_R (μm y^{-1})	η
0	25	-741	330	770	------
	30	-751	260	990	------
	35	-754	210	1220	------
	40	-758	165	1555	------
	45	-769	145	1770	------
1.4	25	-731	600	425	45
	30	-746	440	580	42
	35	-754	325	780	36
	40	-760	220	1175	24
	45	-764	190	1350	23
2.7	25	-727	1000	270	67
	30	-741	790	320	67
	35	-739	600	425	65
	40	-758	420	605	61
	45	-761	340	750	58
8.2	25	-683	2820	80	88
	30	-676	2085	120	88
	35	-695	2125	120	90
	40	-699	1840	140	91
	45	-700	1740	150	92
13.6	25	-625	16660	15	98
	30	-653	12535	20	98
	35	-657	11020	23	98
	40	-649	10800	24	98
	45	-666	9030	28	99
27.2	25	-615	21880	12	98
	30	-631	17910	14	99
	35	-635	17045	15	99
	40	-644	13430	19	99
	45	-656	12555	20	99
54.4	25	-602	33170	8	99
	30	-620	26240	10	99
	35	-628	23870	11	99
	40	-631	20495	13	99
	45	-657	17175	15	99

Table 2: Thermodynamic parameters for the adsorption of AAOA in CO_2 saturated solution on mild steel electrodes at different temperatures.

Temperature (°C)	K_{ads} (1.10^5 M^{-1})	a	R^2	ΔG_{ads}^0 (kJ mol^{-1})
25	4.00	0.46	0.998	-41.9
30	2.90	0.71	0.998	-41.8
35	2.00	0.98	0.996	-41.5
40	1.40	1.02	0.990	-41.3
45	1.02	1.40	0.988	-41.1

Table 3: Electrochemical parameters calculated from polarization measurements on mild steel electrode in CO_2 saturated solution with various inhibitor concentrations at 25, 35 and 45°C.

C (µmol dm^{-3})	Temperature (°C)	j_{corr} (µA cm^{-2})	C_R (µm y^{-1})	η
0	25	65	750	------
	35	76	880	------
	45	105	1215	------
1.4	25	38	440	41
	35	52	610	31
	45	87	1010	17
2.7	25	25	290	61
	35	35	400	54
	45	50	580	52
8.2	25	6.3	75	90
	35	7.8	90	90
	45	9.3	110	91
13.6	25	1.3	16	98
	35	1.7	20	98
	45	1.6	18	99
27.2	25	0.79	9	99
	35	1.1	13	99
	45	1.6	18	99
54.4	25	0.45	5	99
	35	0.91	12	99
	45	1.4	16	99

Table 4: Circuit parameters of the modeling of impedance spectra for mild steel in CO_2 solution containing various concentrations of the inhibitor at different temperatures. C (μmol dm^{-3}), T (ºC), R ($\Omega\ cm^2$), Y_{CPE} ($\Omega^{-1}cm^{-2}s^n10^{-6}$), η.

C	T	R_s	Y_{CPE2}	n_{CPE2}	R_2	Y_{CPE1}	n_{CPE1}	R_1	Y_{CPEdl}	n_{CPEdl}	R_{ct}	η
0	25	3.3	-	-	-	-	-	-	465	0.85	310	-
	35	3.5	-	-	-	-	-	-	655	0.83	200	-
	45	3.1	-	-	-	-	-	-	720	0.82	160	-
2.7	25	3.6	-	-	-	308	0.79	6.1	140	0.87	1005	66
	35	3.4	-	-	-	92	0. 78	5.42	185	0.80	565	65
	45	2. 7	-	-	-	32	0.88	1.04	580	0. 78	400	60
8.2	25	3.3	-	-	-	41	0.82	12.6	165	0.85	3235	90
	35	2.8	-	-	-	74	0. 78	5.46	170	0.93	1720	89
	45	3.5	-	-	-	42	0. 78	5.19	185	0.9	1470	89
13.6	25	3.3	11.7	0.91	10.6	36	1	81.9	175	0.88	12945	98
	35	3.2	5.11	0.96	11.8	13.8	1	73	180	0.82	5340	97
	45	2.9	4.65	0.98	9.01	7.85	1	68	180	0.83	4740	97
27.2	25	3.4	11.1	0.90	18.4	35	1	109	172	0.86	17004	99
	35	3.2	7.11	0.96	17.4	26.9	1	57.8	172	0.80	15750	99
	45	2.4	5.85	0.95	10.9	11.9	1	17.4	232	0.82	6713	98
54.4	298	3.5	7.3	0.93	34.8	35	1	270	147	0.88	32543	99
	308	2.9	7.4	0.93	31.0	38	1	146	151	0.76	19442	99
	45	2.3	7.8	0.94	11.7	19	1	57	200	0.73	10080	98

Table 5: Circuit diffusion parameters from the modeling of impedance spectra for mild steel in a CO_2 solution containing various concentrations of the inhibitor at different temperatures.

C (μmol dm^{-3})	T (^{o}C)	T_{W2} (s)	R_{W2} (Ω cm^2)	T_{W1} (s)	R_{W1} (Ω cm^2)
8.2	25	-	-	15.7	895
	35	-	-	13	725
	45	-	-	8.22	405
13.6	25	0.56	545	17.4	3270
	35	0.024	155	27	5340
	45	0.021	145	14	2030
27.2	25	0.75	783	24.2	6818
	35	0.64	802	21.4	6868
	45	0.60	1059	19.5	3277
54.4	25	1.68	1760	34.6	14230
	35	1.45	2045	30.4	11070
	45	1.2	1150	27.8	4015

Table 6: Corrosion activation parameters derived from Arrhenius and transition state plots for the steel electrode in CO_2 saturated solution with different inhibitor concentrations.

C (μmol dm^{-3})	E_{act} (kJ mol^{-1})	R^2
0	33.4	0.991
0.7	42.6	0.990
1.4	47.7	0.982
2.7	45.1	0.989
8.2	35.8	0.988
13.6	23.0	0.993
27.2	21.1	0.988
40.8	23.4	0.983
54.4	25.2	0.991

Research highlights

Behaviour of N-[2-[(2-aminoethyl)amino]ethyl]-9-octadecenamide (AAOA) as CO_2 corrosion inhibitor.
The adsorption of the AAOA corrosion inhibitor obeys a Frumkin adsorption isotherm.
The inhibition efficiency of the AAOA depends on temperature and concentration.
There is a change in the adsorption mode of the inhibitor with concentration.
AAOA is mainly physi- or chemisorbed for low or high concentrations, respectively.